INTERNATIONAL JOURNAL FOR NUMERICAL AND ANALYTICAL METHODS IN GEOMECHANICS
Int. J. Numer. Anal. Meth. Geomech. 2016; **40**:568–582
Published online 27 July 2015 in Wiley Online Library (wileyonlinelibrary.com). DOI: 10.1002/nag.2416

Embedded beam element with interaction surface for lateral loading of piles

Diego F. Turello[1], Federico Pinto[2,*,†] and Pablo J. Sánchez[3,4]

[1]*FCEFyN UNC-FRSF UTN-CONICET, Santa Fe, Argentina*
[2]*FCEFyN UNC, IDIT UNC-CONICET, Casilla de Correo 916, CP 5000 Córdoba, Argentina*
[3]*CIMEC-UNL-CONICET, Güemes 3450, CP 3000 Santa Fe, Argentina*
[4]*GIMNI-UTN-FRSF, Lavaisse 610, CP 3000 Santa Fe, Argentina*

SUMMARY

This paper presents a numerical formulation of a three dimensional embedded beam element for the modeling of piles, which incorporates an explicit interaction surface between soil and pile. The formulation is herein implemented for lateral loading of piles but is able to represent soil–pile interaction phenomena in a general manner for different types of loading conditions or ground movements. The model assumes perfect adherence between beam and soil along the interaction surface. The paper presents a comparison of the results obtained by means of the present formulation and by means of a previously formulated embedded pile element without interaction surface, as well as reference semi-analytical solutions and a fully 3D finite element (FE) model. It is seen that the proposed embedded element provides a better convergence behavior than a previously formulated embedded element and is able to reproduce key features of a full 3D FE model.

Received 4 March 2015; Revised 16 June 2015; Accepted 23 June 2015

KEY WORDS: embedded beam; finite element; lateral loading; soil–pile interaction

1. INTRODUCTION

The analysis of lateral loading of piles can be performed by means of several techniques with increasing complexity: from simple two dimensional beam over elastic foundation theory to very refined three dimensional (3D) finite element (FE) models.

One of the first approaches proposed in order to model pile–soil interaction phenomena was the Winkler hypothesis, which considers the soil reactions as proportional to the pile displacements by means of independent linear springs distributed along the pile [1]. This method neglects the shear stresses that would develop in the ground because of shear strains. The stiffness of the springs is often referred to as coefficient of subgrade reaction, and it depends on both soil and pile material properties, pile shape, and type of loading (e.g., [2]).

Pasternak [3] and Vlasov [4] independently developed a beam on elastic foundation theory on the basis of two-parameter springs to characterize soil reactions, accounting for shear stresses. These parameters, however, are not widely used in engineering practice, and their definition is not straightforward, as it depends on the assumed displacement field perpendicular to the pile axis [5]. Because the fact that distortions are accounted for in this formulation, special boundary conditions are required at the end of the beam elements in order to represent the shear depression zone [5].

*Correspondence to: Federico Pinto, FCEFyN UNC, IDIT CONICET, Casilla de Correo 916, Av. Velez Sarsfield 1611, Córdoba, Argentina.
†E-mail: fpinto@efn.uncor.edu

By means of a boundary element formulation, Poulos [6] studied the response of piles in homogeneous continua. Poulos tabulated the solutions in several charts in terms of influence factors.

Randolph [7] performed parametric FE analyses on a single vertical pile, subjected to lateral loads and moments applied at the pile head. Results are tabulated in terms of dimensionless parameters that were fitted by Randolph to simple analytical expressions. Randolph considered both homogenous and Gibson (i.e., linearly increasing stiffness with depth) soils.

Although these approaches have been very useful in engineering practice, their application is not straightforward for the analysis of complex soil–structure interaction problems, with large pile groups, heterogeneous soils, and demands both due to applied loads and ground movements.

Sadek and Shahrour [8] proposed an embedded beam element (EBE) formulation for the elastic analysis of piles in FE models, where the pile displacement field is written in terms of the displacement interpolation of the solid (soil) elements. This formulation, however, presents a mechanical incompatibility, which produces non-convergent solutions when the pile nodes are close to or at the solid nodes. This is primarily a consequence of the fact that there is no explicit interaction surface between soil and pile, thus leading to stress singularities when the mesh is further refined. Engin *et al*. [10] show that the results obtained by means of the standard EBE for nonlinear problems depend upon the mesh size of the model because of numerical instability. In order to overcome this issue, Engin *et al*. [10] define an elastic region around the pile axis where the solid Gauss points are forced to remain elastic. Engin *et al*. ([11] and [12]) used this modified EBE formulation to estimate pile group behavior.

This paper presents a novel formulation of an EBE. The model explicitly introduces a finite interaction interface in correspondence with the lateral surface of the pile, here denoted as Ω, where interaction forces, defined in terms of distributed forces, are accounted for within well-posed mechanical framework.

The paper is organized as follows: Section 2 summarizes the standard EBE methodology; in Section 3, discusses the proposed EBE formulation with special emphasis on its implementation; in Section 4, the numerical performance of the proposed formulation is assessed and compared against alternative approaches, such as a semi-analytical formula, the standard EBE method, and a full 3D FE model. The conclusions of this paper are summarized in Section 5.

Throughout the document, lowercase and uppercase letters identify objects defined at the FE level and global (or assembled) level, respectively. Boldface letter is used to denote vector and matrices. Finally, the hat-symbol over any variable implies nodal parameters.

2. STANDARD EMBEDDED BEAM ELEMENT FORMULATION

Figure 1 shows a layout of a standard EBE. The EBE is defined by means of a 3D beam element, writing the displacement DOFs of the beam nodes (i.e., nodes i and j) in terms of the nodal displacements of a 3D solid element.

The standard EBE formulation, originally proposed by Sadek and Shahrour [8], assumes that the displacement field along the beam axis, $\boldsymbol{u_b}$, can be defined by means of standard interpolation

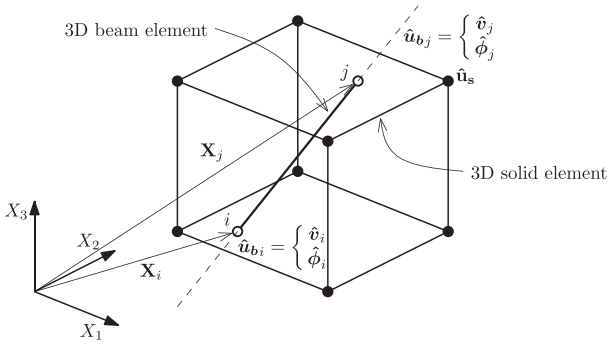

Figure 1. Layout of standard embedded beam element.

DOI: 10.1002/nag

functions in terms of nodal displacements and rotations (6 DOFs per node). The nodal displacements of the beam are then expressed in terms of the solid displacements at the locations of the beam nodes ($\mathbf{X}_i$ and $\mathbf{X}_j$) by means of the solid interpolation scheme. Thus, compatibility is only enforced in terms of displacements at the beam nodes, whereas the displacements within the solid and beam elements are generally non-compatible.

Compatibility at the beam nodes (Figure 1) can be written for the standard EBE as:

$$\begin{aligned} \hat{\boldsymbol{v}}_i &= \mathbf{n_s}(\mathbf{X}_i)\ \hat{\mathbf{u}}_\mathbf{s} \\ \hat{\boldsymbol{v}}_j &= \mathbf{n_s}(\mathbf{X}_j)\ \hat{\mathbf{u}}_\mathbf{s}, \end{aligned} \tag{1}$$

where $\hat{\boldsymbol{v}}_i$ and $\hat{\boldsymbol{v}}_j$ are the beam nodal displacements at the i and j nodes, $\hat{\mathbf{u}}_\mathbf{s}$ are the solid nodal displacements, and $\mathbf{n_s}$ is the matrix containing the standard interpolation functions for the solid FE (Figure 1).

In the standard EBE formulation, the rotational DOFs, $\boldsymbol{\phi}$, are not linked to the solid displacements, and they remain as additional unknowns in the model.

The nodal beam displacements, $\hat{\boldsymbol{u}}_{\boldsymbol{b}}$, are thus written as a function of the nodal solid displacements, $\hat{\mathbf{u}}_\mathbf{s}$, as follows:

$$\hat{u}_b = \begin{pmatrix} \hat{v}_i \\ \hat{\phi}_i \\ \hat{v}_j \\ \hat{\phi}_j \end{pmatrix} = \mathbf{n_{bs}} \begin{pmatrix} \hat{u}_s \\ \hat{\phi}_i \\ \hat{\phi}_j \end{pmatrix}, \tag{2}$$

where $\mathbf{n_{bs}}$ is given by:

$$\mathbf{n_{bs}} = \begin{pmatrix} \mathbf{n_s}(\mathbf{X}_i) & 0\ 0 \\ 0 & \mathrm{I}\ 0 \\ \mathbf{n_s}(\mathbf{X}_j) & 0\ 0 \\ 0 & 0\ \mathrm{I} \end{pmatrix}, \tag{3}$$

where I is a 3×3 identity matrix and 0 represents a null matrix. The elemental transformation matrix $\mathrm{n_{bs}}$, can be assembled into the global transformation matrix $\mathrm{N_{bs}}$, which takes into consideration all beam and soil DOFs.

The global stiffness matrix of the beam elements, $\boldsymbol{K_b}$, is then written in terms of solid nodal displacements, by means of the global transformation matrix $\mathrm{N_{bs}}$, and it is denoted as, $\mathrm{K_{bs}}$:

$$\mathrm{K_{bs}} = \mathrm{N_{bs}}^T\ \boldsymbol{K_b}\ \mathrm{N_{bs}} \tag{4}$$

Thus, the stiffness matrix for the complete set of EBEs is obtained by adding to the stiffness matrix $\mathbf{K_{bs}}$, given by Equation 4, the contributions of the classical solid FE global matrix, $\mathbf{K_s}$, only over the corresponding displacement DOFs.

It should be noted that the nodal beam forces are transformed into equivalent nodal solid forces in order to perform the final assembly of the problem. Thus, the equivalent force vector in terms of solid DOFs, $\hat{\mathbf{P}}_{\mathbf{bs}}$, can be expressed as a function of the vector in terms of beam DOFs, $\hat{\boldsymbol{P}}_{\boldsymbol{b}}$, by means of the transformation matrix $\mathbf{N_{bs}}$, as follows:

$$\hat{\mathbf{P}}_{\mathbf{bs}} = \mathbf{N_{bs}}^T\ \hat{\boldsymbol{P}}_{\boldsymbol{b}}. \tag{5}$$

In this formulation, the nodal moment loads in the beam remain as beam nodal loads and do not contribute to the solid load vector (Equation (5)). This is a direct consequence of the fact that the rotational DOFs of the beam are independent of the solid displacements field and remain as

DOI: 10.1002/nag

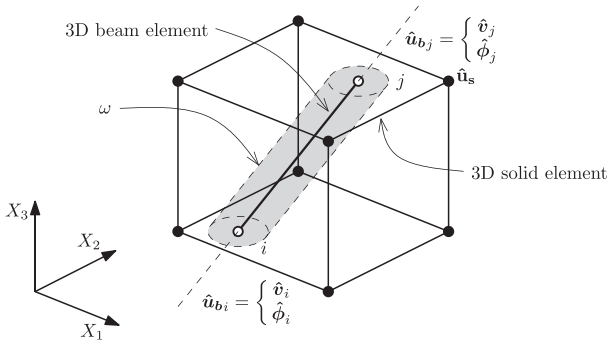

Figure 2. Layout of proposed embedded beam element.

additional unknown parameters. Only the translational DOFs and forces in the beam are transformed into equivalent solid DOFs and assembled with the solid elements.

Given the fact that the formulation does not consider an explicit interaction surface between beam and solid, the solid–beam interaction forces tend to be distributed over a line, generating infinite stresses in the solid adjacent to the beam for decreasing mesh sizes.

3. PROPOSED EMBEDDED BEAM ELEMENT FORMULATION

In order to overcome the limitations of the standard EBE formulation described earlier, a novel EBE with explicit interaction surface is proposed in this paper. Figure 2, shows a sketch of the proposed EBE with explicit interaction surface.

The main purpose of this improved EBE formulation is to explicitly represent the force interactions at the pile surface in order to overcome singular stresses. From the mechanical point of view, this is naturally achieved by imposing the compatibility between beam and solid displacements along the interaction surface. That is, the system of interaction forces can be viewed as the system of reactive forces due to the kinematical restriction imposed at the interaction surface.

As a starting point of this formulation, beam and solid displacements are defined by means of standard interpolation functions on the basis of nodal displacements (beam and solid) and rotations (beam only). Mapping functions are defined in order to express the beam displacements $\mathbf{u_b}$ and forces $\mathbf{f_b}$, at the interaction surface, as a function of the beam displacements $\boldsymbol{u_b}$ and forces $\boldsymbol{f_b}$ defined along the beam axis, respectively.

3.1. Discretization and mapping functions

The 3D solid displacement vector field $\mathbf{u_s}$ is discretized by means of standard interpolation functions, $\mathbf{n_s}$, in terms of the spatial position, $\mathbf{X}$, and nodal parameters, $\hat{\mathbf{u}}_\mathbf{s}$:

$$\mathbf{u_s}(\mathbf{X}) = \mathbf{n_s}(\mathbf{X})\ \hat{\mathbf{u}}_\mathbf{s}. \tag{6}$$

The beam displacement vector field at the interaction surface $\mathbf{u_b}$ (Figure 3) is expressed as a function of the beam nodal displacements $\hat{\boldsymbol{u}}_{\boldsymbol{b}}$ (displacements and rotations), by means of a mapping matrix $\mathbf{h_u}$, which is composed of: (i) an interpolation matrix $\boldsymbol{n_u}$ that defines the displacement field at the beam axis in terms of nodal displacements $\hat{\boldsymbol{u}}_{\boldsymbol{b}}$, and (ii) a matrix $\mathbf{m_u}$ that converts displacements and rotations at the beam axis into a vector displacement field at the interaction surface.

Figure 3 shows a layout of the mapping operations, together with the global (i.e., X_1, X_2, X_3) and local (i.e., r, φ) coordinate systems for the case of a vertical pile with circular cross section (R_p is the radius of the pile). While the procedure can be generalized for other cases, this is not a straightforward task, as a new generalized mapping operator needs to be defined.

DOI: 10.1002/nag

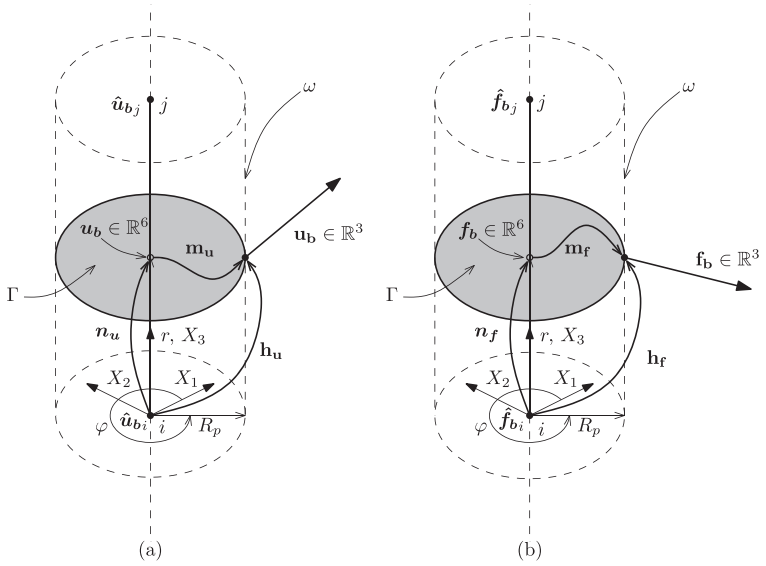

Figure 3. Layout of mapping matrices (a) $\mathbf{h_u}$ and (b) $\mathbf{h_f}$ in the proposed embedded beam element.

The interpolation matrix for beam displacements, $\boldsymbol{n_u}$, is defined in terms of the local position along the beam axis, r (Figure 3).

The mapping matrix $\mathbf{m_u}$ is defined in terms of the local cylindrical coordinate, φ, and takes into account the standard Navier–Bernoulli hypothesis, where the beam cross section Γ, remains planar, undeformed, and perpendicular to the beam axis. This hypothesis may be inaccurate for piles in stiff soils, where shear deformations may be significant because of the short characteristic length. However, the coupling formulation technique herein discussed remains valid if shear strains are accounted for and will be implemented in future developments.

The beam displacement vector field, $\mathbf{u_b}$, at the interaction surface, can thus be written in terms of the beam nodal displacements, $\hat{\boldsymbol{u}}_{\boldsymbol{b}}$, as:

$$\mathbf{u_b}(r,\varphi) = \mathbf{h_u}(r,\varphi)\ \hat{\boldsymbol{u}}_{\boldsymbol{b}} = \mathbf{m_u}(\varphi)\ \boldsymbol{n_u}(r)\ \hat{\boldsymbol{u}}_{\boldsymbol{b}}. \tag{7}$$

The explicit form of the mapping matrix, $\mathbf{h_u}$, for a 2-node (i.e., nodes i and j) cylindrical pile in local coordinates, as it is shown in Figure 3, is given in Equation 8.

$$\begin{aligned}
&\mathbf{h_u}(r,\varphi) = \mathbf{m_u}(\varphi)\ \boldsymbol{n_u}(r)\\
&\boldsymbol{n_u}(r) = \left(\boldsymbol{n_{ui}}(r)\ \boldsymbol{n_{uj}}(r)\right)\\
&\text{with}\\
&\boldsymbol{n_{ui}}(r) = \begin{pmatrix}
n^H_{1i}(r) & 0 & 0 & 0 & n^H_{2i}(r) & 0\\
0 & n^H_{1i}(r) & 0 & n^H_{2i}(r) & 0 & 0\\
0 & 0 & n^L_i(r) & 0 & 0 & 0\\
0 & -n^H_{1i,r}(r) & 0 & -n^H_{2i,r}(r) & 0 & 0\\
n^H_{1i,r}(r) & 0 & 0 & 0 & n^H_{2i,r}(r) & 0\\
0 & 0 & 0 & 0 & 0 & n^L_i(r)
\end{pmatrix}\\
&\mathbf{m_u}(\varphi) = \begin{pmatrix}
1\ 0\ 0 & 0 & 0 & -R_p\sin(\varphi)\\
0\ 1\ 0 & 0 & 0 & R_p\cos(\varphi)\\
0\ 0\ 1 & R_p\sin(\varphi) & -R_p\cos(\varphi) & 0
\end{pmatrix},
\end{aligned} \tag{8}$$

DOI: 10.1002/nag

where n_1^H, n_2^H are the cubic Hermite polynomial functions for interpolation of displacements in terms of nodal displacements and rotations, respectively; n^L are the standard linear interpolation functions, and $\boldsymbol{n}_{\boldsymbol{u}\,j}(r)$ has an identical expression to $\boldsymbol{n}_{\boldsymbol{u}i}(r)$ but exchanging the sub-index i by j. In this equation, $()_{,r}$ represents the partial derivative with respect to the local coordinate r.

Similarly, the interaction force field $\mathbf{f_b}$, at the interaction surface, can be expressed as a function of nodal beam interaction forces, $\hat{\boldsymbol{f}}_{\boldsymbol{b}}$, by means of the mapping matrix $\mathbf{h_f}$. The mapping scheme consists of two parts: (i) a matrix $\boldsymbol{n}_{\boldsymbol{f}}$ that performs an interpolation of the beam forces $\boldsymbol{f}_{\boldsymbol{b}}$ defined at the beam axis in terms of nodal force values $\hat{\boldsymbol{f}}_{\boldsymbol{b}}$, and (ii) a matrix $\mathbf{m_f}$ that defines the distributed force vector field $\mathbf{f_b}$, at the interaction surface, in terms of the forces interpolated at the beam axis $\boldsymbol{f}_{\boldsymbol{b}}$.

The interpolation matrix $\boldsymbol{n}_{\boldsymbol{f}}$ is written in terms of the local coordinate r (Figure 3), whereas the matrix $\mathbf{m_f}$, which transfers the loads from the beam axis into the interaction surface, is defined in terms of the local coordinate φ.

The distributed force vector field $\mathbf{f_b}$, at the interaction surface, can thus be written as:

$$\mathbf{f_b}(r,\varphi) = \mathbf{h_f}(r,\varphi)\ \hat{\boldsymbol{f}}_{\boldsymbol{b}} = \mathbf{m_f}(\varphi)\ \boldsymbol{n}_{\boldsymbol{f}}(r)\ \hat{\boldsymbol{f}}_{\boldsymbol{b}}. \tag{9}$$

The explicit form of the mapping function $\mathbf{h_f}$ for a cylindrical pile is given in Equation 10.

$$\begin{aligned}
&\mathbf{h_f}(r,\varphi) = \mathbf{m_f}(\varphi)\ \boldsymbol{n}_{\boldsymbol{f}}(r)\\
&\boldsymbol{n}_{\boldsymbol{f}}(r) = \left(\boldsymbol{n}_{\boldsymbol{f}\,i}(r)\ \boldsymbol{n}_{\boldsymbol{f}\,j}(r)\right)\\
&\text{with}\\
&\boldsymbol{n}_{\boldsymbol{f}\,i}(r) = \begin{pmatrix}
n_{1\,i}^H(r) & 0 & 0 & 0 & n_{2\,i}^H(r) & 0\\
0 & n_{1\,i}^H(r) & 0 & n_{2\,i}^H(r) & 0 & 0\\
0 & 0 & n_i^L(r) & 0 & 0 & 0\\
0 & -n_{1\,i,r}^H(r) & 0 & -n_{2\,i,r}^H(r) & 0 & 0\\
n_{1\,i,r}^H(r) & 0 & 0 & 0 & n_{2\,i,r}^H(r) & 0\\
0 & 0 & 0 & 0 & 0 & n_i^L(r)
\end{pmatrix}\\
&\mathbf{m_f}(\varphi) = \begin{pmatrix}
\dfrac{1}{2\pi R_p} & 0 & 0 & 0 & 0 & -\dfrac{\sin(\varphi)}{2\pi R_p^2}\\
0 & \dfrac{1}{2\pi R_p} & 0 & 0 & 0 & \dfrac{\cos(\varphi)}{2\pi R_p^2}\\
0 & 0 & \dfrac{1}{2\pi R_p} & \dfrac{\sin(\varphi)}{\pi R_p^2} & -\dfrac{\cos(\varphi)}{\pi R_p^2} & 0
\end{pmatrix}
\end{aligned} \tag{10}$$

It should be noted that the interpolation matrices $\boldsymbol{n}_{\boldsymbol{u}}$ and $\boldsymbol{n}_{\boldsymbol{f}}$ are defined in terms of the r coordinate alone (Figure 3), whereas the mapping functions $\mathbf{h_u}$ and $\mathbf{h_f}$ are written in terms of the local cylindrical coordinates r and φ.

Figure 4 shows a sketch of the interaction force patterns for different loading modes (i.e., axial and transverse loading, bending, and torsion).

3.2. Formulation of the embedded beam element with interaction surface

Compatibility of solid and beam displacements is defined at the interaction surface Ω. In this paper, a *fully rough* elastic interaction is considered. However, the formulation can readily be extended to incorporate more realistic pile–soil interaction, accounting for nonlinear behavior (material and slippage). A weak kinematic compatibility is enforced by imposing that the relative displacement between beam and soil, at the interaction surface, produces no virtual work with respect to any

DOI: 10.1002/nag

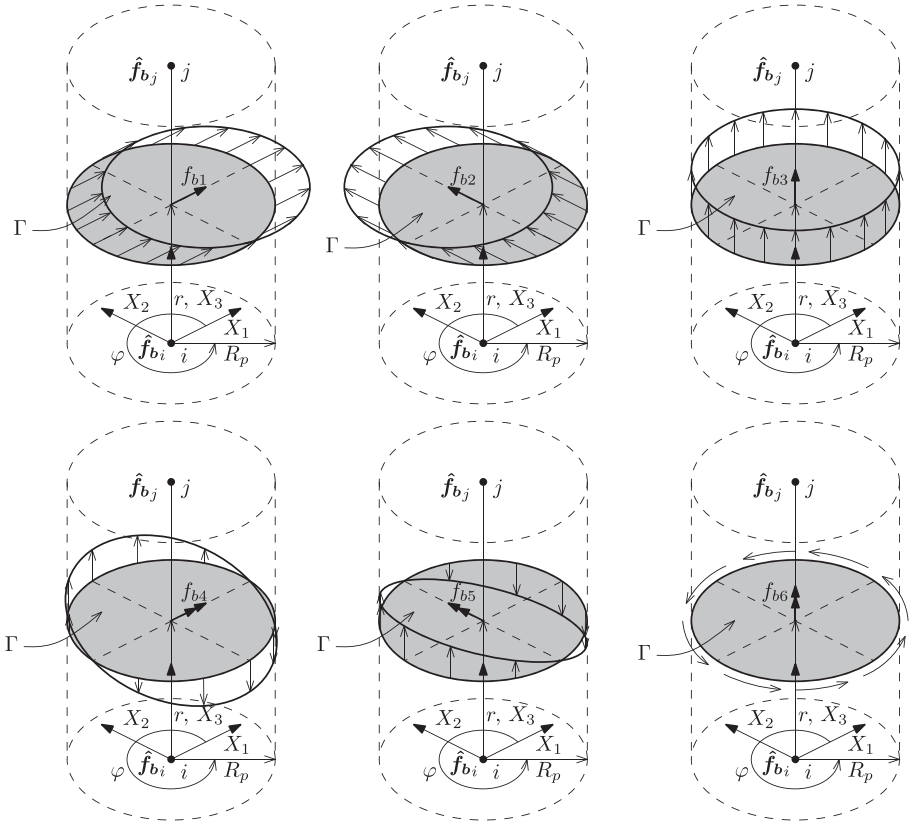

Figure 4. Interaction force patterns for different types of loads.

admissible system of virtual interaction forces, $\delta\mathbf{f_b}$ (this vector field at global level is written as $\delta \boldsymbol{F_b}$). Using FEM, this restriction is expressed as:

$$
\begin{aligned}
0 &= \mathop{\mathbf{A}}_{e=1}^{e=N_b} \int_{\omega} \delta\mathbf{f_b}^T \ (\mathbf{u_s} - \mathbf{u_b}) \ \mathrm{d}\omega \qquad \forall \qquad \text{admissible } \delta\mathbf{f_b}^T \\
0 &= \delta\hat{\boldsymbol{F}}_{\boldsymbol{b}}^{\ T} \underbrace{\mathop{\mathbf{A}}_{e=1}^{e=N_b} \int_{\omega} \mathbf{h_f}^T \ \mathbf{n_s} \ \mathrm{d}\omega}_{\mathbf{A}^T} \hat{\mathbf{U}}_{\mathbf{s}} - \delta\hat{\boldsymbol{F}}_{\boldsymbol{b}}^{\ T} \underbrace{\mathop{\mathbf{A}}_{e=1}^{e=N_b} \int_{\omega} \mathbf{h_f}^T \ \mathbf{h_u} \ \mathrm{d}\omega}_{\mathbf{B}^T} \hat{\boldsymbol{U}}_{\boldsymbol{b}} \qquad \forall \qquad \delta\hat{\boldsymbol{F}}_{\boldsymbol{b}}^{\ T} \\
0 &= \mathbf{A}^T \ \hat{\mathbf{U}}_{\mathbf{s}} - \mathbf{B}^T \ \hat{\boldsymbol{U}}_{\boldsymbol{b}},
\end{aligned}
\tag{11}
$$

where $\hat{\mathbf{U}}_{\mathbf{s}}$ is the assembled vector of all solid DOFs and $\hat{\boldsymbol{U}}_{\boldsymbol{b}}$ is the assembled vector of all nodal beam DOFs, $\mathbf{A}$ is a proper FE assembly operator; N_b is the number of beam elements, and the global matrices $\mathbf{A}$ and $\mathbf{B}$ are defined as:

$$
\begin{aligned}
\mathbf{A} &= \mathop{\mathbf{A}}_{e=1}^{e=N_b} \int_{\omega} \mathbf{n_s}^T \ \mathbf{h_f} \ \mathrm{d}\omega \\
\mathbf{B} &= \mathop{\mathbf{A}}_{e=1}^{e=N_b} \int_{\omega} \mathbf{h_u}^T \ \mathbf{h_f} \ \mathrm{d}\omega.
\end{aligned}
\tag{12}
$$

If the same interpolation matrices for both $\boldsymbol{u_b}$ and $\boldsymbol{f_b}$ are chosen (i.e., $\boldsymbol{n_u} = \boldsymbol{n_f}$), the matrix $\mathbf{B}$ yields invertible. Thus, the nodal beam displacements could be expressed in terms of nodal solid displacements as:

$$
\hat{\boldsymbol{U}}_{\boldsymbol{b}} = \mathbf{B}^{-T} \ \mathbf{A}^T \ \hat{\mathbf{U}}_{\mathbf{s}}. \tag{13}
$$

DOI: 10.1002/nag

By establishing the virtual work equilibrium under virtual nodal displacement field of the entire pile, $\delta\hat{\boldsymbol{U}}_{\boldsymbol{b}}$, and using Equations 7 and 9, the equivalent lumped load vector of the complete pile, $\hat{\boldsymbol{P}}_{\boldsymbol{b}}$, can be written in terms of the nodal interaction forces vector, $\hat{\boldsymbol{F}}_{\boldsymbol{b}}$, as:

$$\begin{aligned} \delta\hat{\boldsymbol{U}}_{\boldsymbol{b}}{}^{T}\ \hat{\boldsymbol{P}}_{\boldsymbol{b}} &= \delta\hat{\boldsymbol{U}}_{\boldsymbol{b}}{}^{T}\ \underset{e=1}{\overset{e=N_b}{\mathbf{A}}} \int_{\omega} \mathbf{h_u}^{T}\ \mathbf{h_f}\ \mathrm{d}\omega\ \hat{\boldsymbol{F}}_{\boldsymbol{b}} \qquad \forall \qquad \delta\hat{\boldsymbol{U}}_{\boldsymbol{b}}{}^{T} \\ \hat{\boldsymbol{P}}_{\boldsymbol{b}} &= \underbrace{\underset{e=1}{\overset{e=N_b}{\mathbf{A}}} \int_{\omega} \mathbf{h_u}^{T}\ \mathbf{h_f}\ \mathrm{d}\omega}_{\mathbf{B}}\ \hat{\boldsymbol{F}}_{\boldsymbol{b}} \end{aligned} \tag{14}$$

$$\hat{\boldsymbol{P}}_{\boldsymbol{b}} = \mathbf{B}\ \hat{\boldsymbol{F}}_{\boldsymbol{b}}. \tag{15}$$

By establishing the virtual work equilibrium under a virtual solid nodal displacements, $\delta\hat{\mathbf{U}}_{\mathbf{s}}$, the interaction load vector defined in terms of the solid DOFs, $\hat{\mathbf{P}}_{\mathbf{s}}$, can be expressed as a function of the global nodal interaction forces vector, $\hat{\boldsymbol{F}}_{\boldsymbol{b}}$, as:

$$\begin{aligned} \delta\hat{\mathbf{U}}_{\mathbf{s}}^{T}\ \hat{\mathbf{P}}_{\mathbf{s}} &= \delta\hat{\mathbf{U}}_{\mathbf{s}}^{T}\ \underset{e=1}{\overset{e=N_b}{\mathbf{A}}} \int_{\omega} \mathbf{n_s}^{T}\ \mathbf{h_f}\ \mathrm{d}\omega\ \hat{\boldsymbol{F}}_{\boldsymbol{b}} \qquad \forall \qquad \delta\hat{\mathbf{U}}_{\mathbf{s}}^{T} \\ \hat{\mathbf{P}}_{\mathbf{s}} &= \underbrace{\underset{e=1}{\overset{e=N_b}{\mathbf{A}}} \int_{\omega} \mathbf{n_s}^{T}\ \mathbf{h_f}\ \mathrm{d}\omega}_{\mathbf{A}}\ \hat{\boldsymbol{F}}_{\boldsymbol{b}} \end{aligned} \tag{16}$$

$$\hat{\mathbf{P}}_{\mathbf{s}} = \mathbf{A}\ \hat{\boldsymbol{F}}_{\boldsymbol{b}}. \tag{17}$$

Using Equation 15, the equilibrium of the beam can hence be written in terms of global nodal interaction forces, $\hat{\boldsymbol{F}}_{\boldsymbol{b}}$, as:

$$\begin{aligned} \boldsymbol{K_b}\ \hat{\boldsymbol{U}}_{\boldsymbol{b}} &= \hat{\boldsymbol{P}}_{\boldsymbol{b}} \\ \boldsymbol{K_b}\ \hat{\boldsymbol{U}}_{\boldsymbol{b}} &= \mathbf{B}\ \hat{\boldsymbol{F}}_{\boldsymbol{b}}, \end{aligned} \tag{18}$$

where $\boldsymbol{K_b}$ is the global standard stiffness matrix for the entire pile. If the same interpolation matrices $\boldsymbol{n_u}$ and $\boldsymbol{n_f}$ are chosen, the matrix $\mathbf{B}$ yields invertible. Thus, the global nodal interaction forces, $\hat{\boldsymbol{F}}_{\boldsymbol{b}}$, can be expressed as:

$$\hat{\boldsymbol{F}}_{\boldsymbol{b}} = \mathbf{B}^{-1}\ \boldsymbol{K_b}\ \hat{\boldsymbol{U}}_{\boldsymbol{b}}. \tag{19}$$

Replacing Equations 19 and 13 into Equation 17, the global beam stiffness matrix can be written in terms of solid DOFs as:

$$\begin{aligned} \hat{\mathbf{P}}_{\mathbf{s}} &= \mathbf{A}\ \hat{\boldsymbol{F}}_{\boldsymbol{b}} \\ \hat{\mathbf{P}}_{\mathbf{s}} &= \mathbf{A}\ \mathbf{B}^{-1}\ \boldsymbol{K_b}\ \hat{\boldsymbol{U}}_{\boldsymbol{b}} \\ \hat{\mathbf{P}}_{\mathbf{s}} &= \underbrace{\mathbf{A}\ \mathbf{B}^{-1}\ \boldsymbol{K_b}\ \mathbf{B}^{-T}\ \mathbf{A}^{T}}_{\mathbf{K_{bs}}}\ \hat{\mathbf{U}}_{\mathbf{s}} \\ \hat{\mathbf{P}}_{\mathbf{s}} &= \mathbf{K_{bs}}\ \hat{\mathbf{U}}_{\mathbf{s}}. \end{aligned} \tag{20}$$

The global stiffness matrix of the beam in terms of solid DOFs, $\mathbf{K_{bs}}$, yields symmetric because of the fact that it inherits the symmetry of the standard beam stiffness matrix. This matrix can readily be assembled to the solid stiffness matrix, in order to obtain the total stiffness matrix of the embedded pile. Both translational and rotational beam DOFs are transformed into equivalent solid DOFs.

The problem is thus solved in terms of solid DOFs, whereas the beam DOFs can be subsequently obtained by means of Equation 13, as a post-process step.

DOI: 10.1002/nag

Using Equations 15 and 17, the global nodal load vector of the beam element, $\hat{\boldsymbol{P}}_{\boldsymbol{b}}$, can be transformed into an equivalent global nodal solid vector load, $\hat{\mathbf{P}}_{\mathbf{bs}}$, as:

$$\hat{\mathbf{P}}_{\mathbf{bs}} = \mathbf{A}\,\mathbf{B}^{-1}\,\hat{\boldsymbol{P}}_{\boldsymbol{b}}. \tag{21}$$

This is of particular relevance for pile loading problems, where external loads and moments are converted to solid forces. Thus, the complete load vector, in terms of solid DOFs, is obtained by adding the contributions of $\hat{\mathbf{P}}_{\mathbf{s}}$, $\hat{\mathbf{P}}_{\mathbf{bs}}$, and the standard lumped load vector due to external forces (e.g., surface traction, and body force) applied in the solid domain.

3.3. Numerical implementation

The proposed EBE formulation is general and can be implemented for several solid and beam element formulations.

In this paper, the formulation is implemented for two types of solid elements: an 8-node bilinear brick element with reduced-integration (referred to as H8) and a 27-node quadratic brick element (referred to as H27). The interpolation functions for both elements belong to the $\mathcal{C}^0$ space [9].

Two pile elements are considered: a 2-node beam element, referred to as B2, with standard Hermite cubic interpolation functions in bending (interpolation functions belong to $\mathcal{C}^1$ space) and standard linear interpolation functions for axial behavior and torsional behavior (interpolation functions belong to $\mathcal{C}^0$ space) as well as a 3-node beam element, referred to as B3, with fifth-order Hermite polynomials in bending (interpolation functions belong to $\mathcal{C}^1$ space) and quadratic interpolation functions for axial and torsional components (interpolation functions belong to $\mathcal{C}^0$ space).

Several combinations of these elements can be made in order to formulate an EBE. For example: H8B2, H27B2, H8B3, and H27B3 EBEs can be generated by means of the solid and beam elements described earlier. In this paper, however, only H8B2 and H27B2 are considered for the examples shown.

The integrals over the interaction surface given in Equation 12 are evaluated by means of numerical integration.

4. VALIDATION

4.1. Reference solutions

Randolph [13] derived a semi-analytical solution for lateral loading of single vertical piles based on FE results. This solution considers an 'active pile length' where displacements are significant. Randolph proposed several curves that represent lateral deflections and bending moments as a function of dimensionless parameters.

In order to obtain an independent benchmark solution, in addition to Randolph's, a full 3D model is solved by means of ABAQUS™[14](see a sketch of the test setting in Figure 8). In this model, both soil and pile domains are modeled by means of 3D solid elements. Two types of solid elements are used: C3D8R 8-node bilinear brick elements and C3D20 20-node biquadratic brick elements, both with reduced integration.

In order to study the convergence of the proposed EBE formulation, with respect to the full 3D ABAQUS™ model, the mesh size in the FEM model is varied from coarse to fine, in order to generate a head displacement, u_{head}, versus mesh size, l_m, curve, which is normalized with respect to the pile diameter D_p. Figure 5 shows the refined mesh used in the analysis.

The external boundaries are set at a $10 \times D_p$ offset from the pile axis, where all displacements components are constrained.

In the ABAQUS™ model, the external load is applied as a uniformly distributed traction force at the upper end of the pile along the $+X$ direction. Both soil and pile are represented by means of linearly elastic, homogeneous, and isotropic materials.

The stresses within the pile cross section, Γ (Figure 3), are integrated in order to obtain the equivalent beam forces (i.e., bending moments and shear forces). Figures 6 and 7 show the

DOI: 10.1002/nag

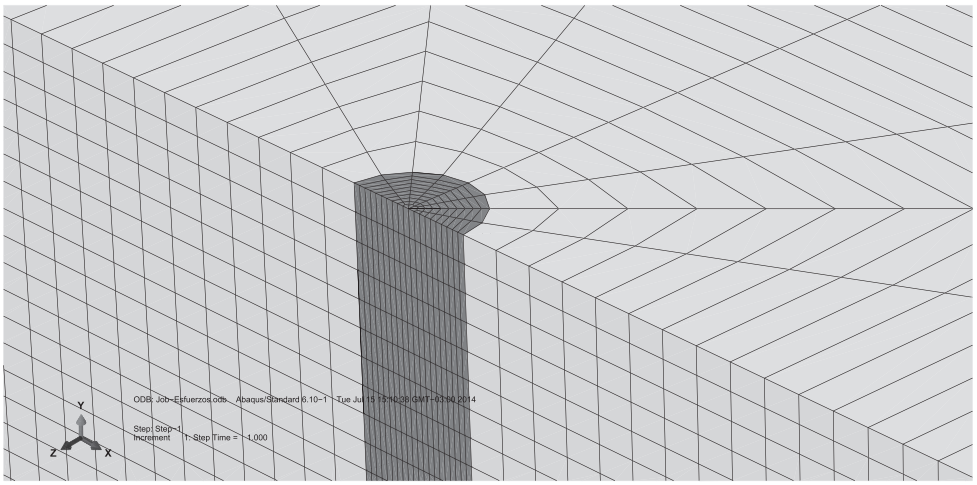

Figure 5. Partial view of the refined mesh used in the ABAQUS™ model.

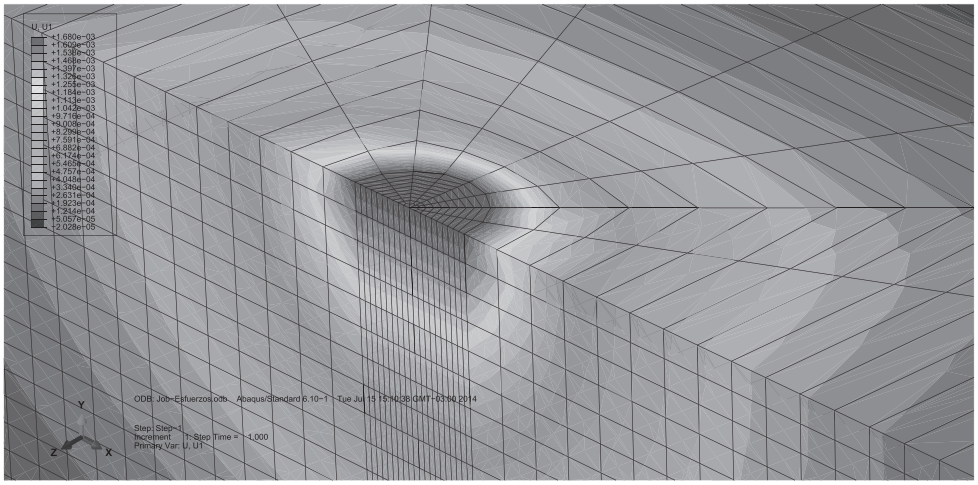

Figure 6. Lateral displacements U_1 (U_X according to global axes in ABAQUS™ model) for the C3D8R.

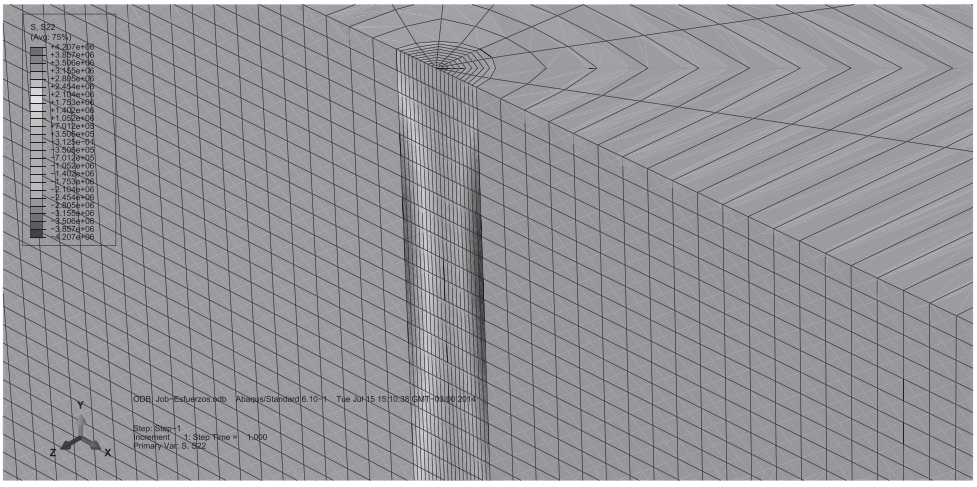

Figure 7. Normal stress S_{22} (S_{YY} according to global axes in ABAQUS™ model) for the C3D8R.

DOI: 10.1002/nag

displacements, U_1 (along global axis X), and the stresses, S_{22} (or S_{YY}, according to the global axis), respectively, for the C3D8R solid element and a fine mesh.

It should be noted that the numerical implementation of the EBE described in this paper does not include shear strains in the beam, which represents a deviation from the full 3D ABAQUS™ model.

4.2. Comparison of results

A comparison of results is drawn on the basis of lateral loading results of a single vertical pile, considering the standard EBE formulation, and the formulation with explicit interaction surface proposed in this paper. Results are benchmarked with respect to Randolph's solution and 3D FEM model results.

The soil is discretized by means of H8 and H27 solid elements, whereas the pile is represented by means of B2 beam elements. Hence, H8B2 and H27B2 EBEs were considered for the soil structure interaction analyses.

The mesh size varies from $l_m = 5.0 \times D_p$ (coarse) to $l_m = 1.0 \times D_p$ (fine). The external load, P, is applied along the $+X_1$ direction at the upper end of the pile (Figure 8).

In this example, the pile and solid nodes are coincident, as shown in Figure 8.

The soil elastic parameters considered for the analysis are: Young's modulus $E_s = 100\,\text{Mpa}$ and Poisson's ratio $\nu_s = 0.33$. On the other hand, the pile elastic properties are: Young's modulus $E_p = 30,000\,\text{Mpa}$, $D_p = 0.50\,\text{m}$, $L_p = 10.00\,\text{m}$. Physical meaning for all these parameters are shown in Figure 8.

Figure 9 shows the convergence behavior of the EBE models. It can be seen that the standard EBE formulation shows non-convergent results for decreasing mesh sizes, for either the H8B2 or H27B2 EBEs. The lack of convergence in the standard EBE formulation is due to the fact that it does not properly represent the actual distribution of interaction forces, thus leading to unrealistically large stresses (and displacements) for decreasing mesh sizes. In the limit where the mesh size tends to zero, the standard EBE formulation yields a line load in a solid, thus leading to unbounded stresses near the pile. It is therefore expected that displacements obtained by means of the standard EBE increase up to values larger than the reference solutions for decreasing mesh sizes l_m.

Figure 9 also shows the convergence behavior of the proposed EBE elements with interaction surface. It is seen that the lateral displacements at the pile head converge to the benchmark solution with decreasing l_m.

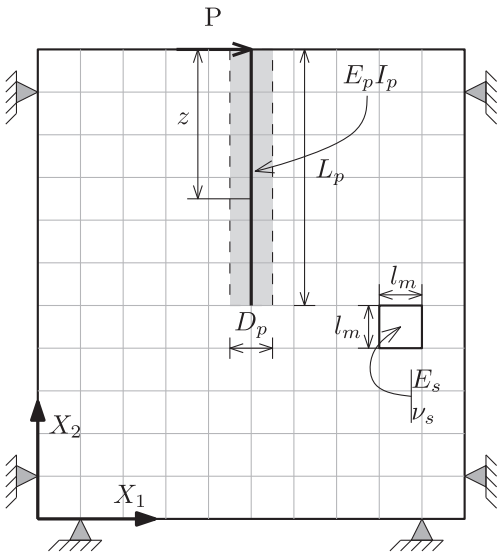

Figure 8. Lateral view of the 3D example.

DOI: 10.1002/nag

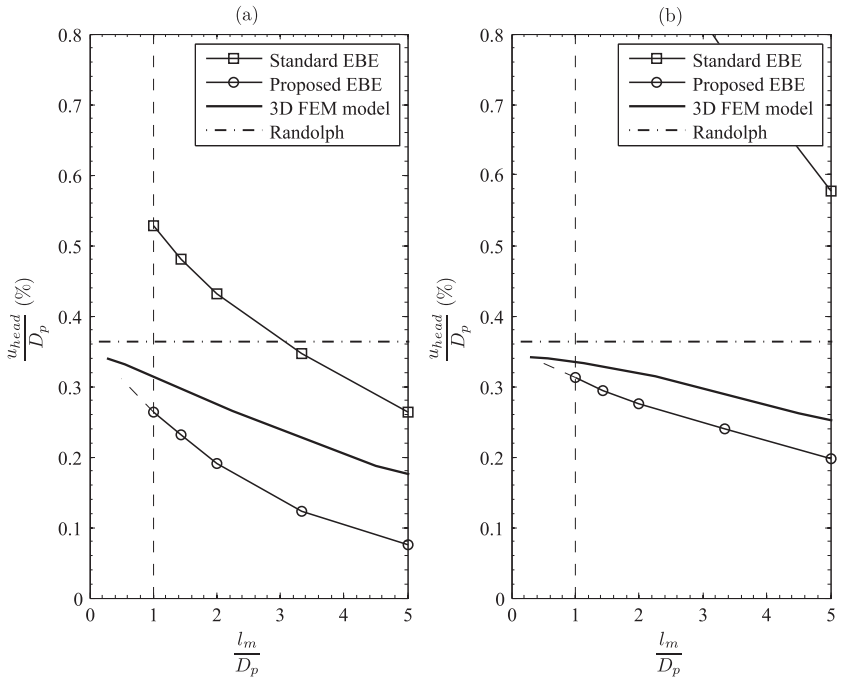

Figure 9. Pile head lateral displacement, u_{head}, for (a) H8B2 and (b) H27B2 embedded beam elements (EBEs).

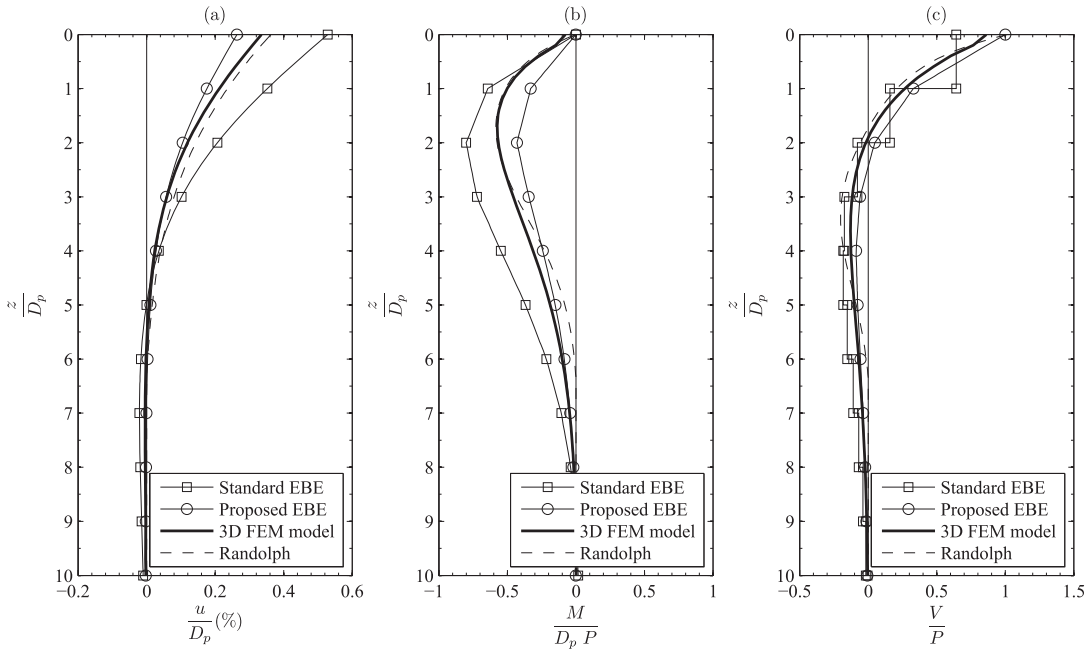

Figure 10. Normalized results for H8B2 embedded beam elements (EBEs) versus normalized depth: (a) lateral deflection u, (b) bending moment M, and (c) shear force V.

It is noted that the proposed EBE shows a slightly stiffer behavior than the 3D FEM model, probably due to the fact that this model accounts for shear strains, whereas the EBE model follows the Euler-Bernoulli hypothesis.

DOI: 10.1002/nag

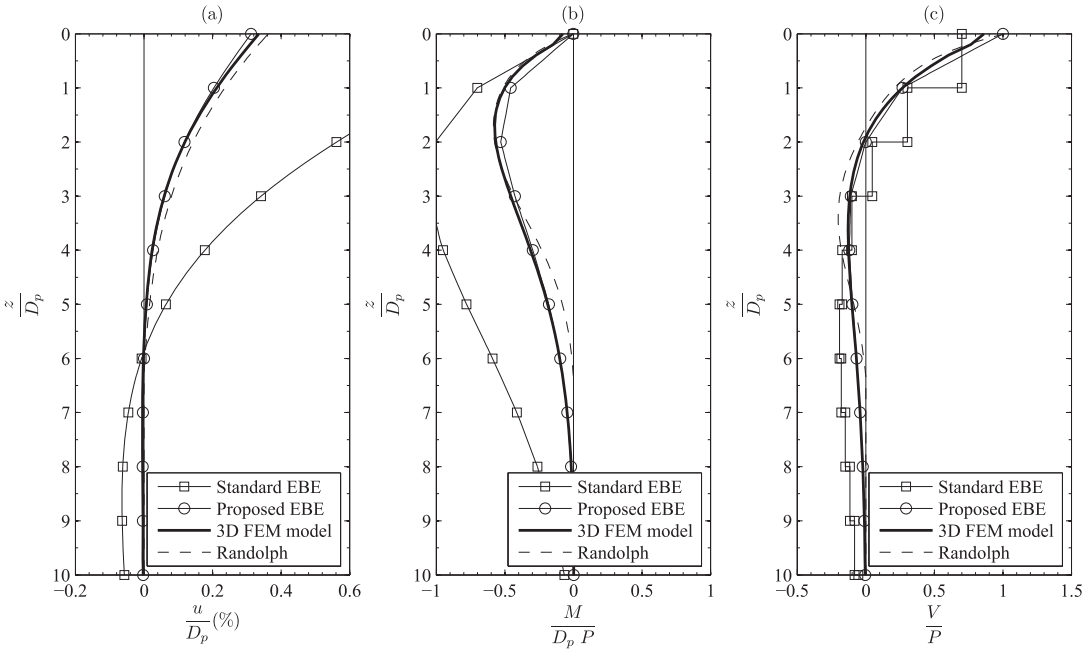

Figure 11. Normalized results for H27B2 embedded beam elements (EBEs) versus normalized depth: (a) lateral deflection u, (b) bending moment M, and (c) shear force V.

Figure 10 and Figure 11 show the normalized EBE model results (i.e., lateral deflection u, bending moments M, and shear forces V) for the H8B2 and H27B2 elements, respectively, as a function of the normalized depth, z/D_p, together with the benchmark solutions.

It is seen that the standard EBE model yields lateral deflections that do not converge to the benchmark solutions. The bending moments and shear forces obtained by means of the standard EBE model are greater than the ones obtained by means of the 3D FEM model and Randolph's solution. This is particularly noticeable for the H27B2 elements, which consider a biquadratic interpolation for the solid elements and a 2-node beam, as shown in Figure 11.

The proposed EBE formulation shows both bending moments and shear forces that converge to the reference solutions, with an acceptable degree of accuracy, when mesh sizes tend to the pile diameter. This is observed for both H8B2 and H27B2 EBEs (Figures 10 and 11), where it is seen that the results obtained by means of the H27B2 element are in remarkable agreement with the reference solutions.

In order to assess the convergence rate, a simple relative error norm is defined as:

$$||e|| = \frac{\int_0^{L_p} \sqrt{\left(u_{ref} - u\right)^2}\,\mathrm{d}z}{\int_0^{L_p} \sqrt{\left(u_{ref}\right)^2}\,\mathrm{d}z}, \tag{22}$$

where u_{ref} is the lateral deflection in the full 3D ABAQUS™ solution for the finer mesh considered in the analysis, u is the lateral deflection obtained with the proposed EBE formulation, and L_p is the pile length. Figure 12 shows the error norm for both H8B2 and H27B2 EBEs considering the standard as well as the proposed formulation.

It is seen that the relative error norm $||e||$ in the standard EBE formulation does not seem to vanish as the mesh size tends to the pile diameter for both H8B2 and H27B2 elements. The proposed EBE formulation, however, shows a relative error norm that essentially vanishes as the mesh size tends to the pile diameter for both elements considered in the example.

It is observed that the convergence rate is greater for the H27B2 element and that the relative error norm is smaller for the H27B2 for all mesh sizes considered in the analyses.

DOI: 10.1002/nag

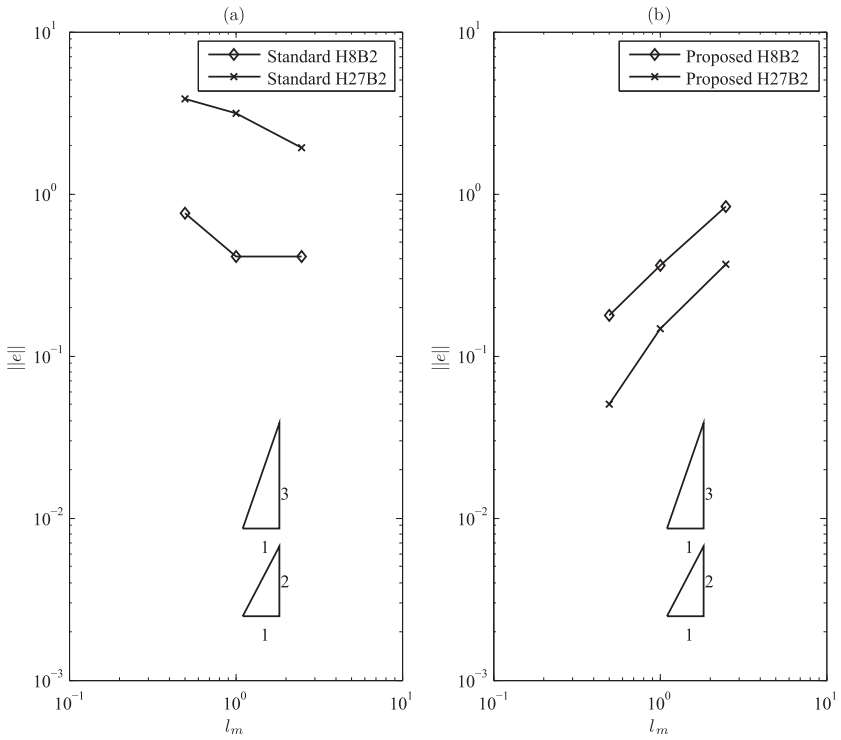

Figure 12. Relative error norm $||e||$ versus l_m. (a) standard embedded beam element (EBE) and (b) proposed EBE.

5. CONCLUSIONS

This paper presents a new formulation for an EBE with an explicit interaction surface where the equilibrium of interaction forces and kinematic compatibility between the soil and beam displacement fields are established. Actually, a family of EBE can be derived from the present methodology, in accordance with the interpolation order adopted for the solid and beam elements.

The kinematics of the beam element (i.e., displacements and rotations), as well as the elemental interaction forces (i.e., distributed forces and moments) are defined by means of mapping functions that allow the evaluation of 3D beam displacement vectors, $\mathbf{u_b}$, and interaction forces, $\mathbf{f_b}$, over the interaction surface, ω. The explicit forms of these mapping functions are given for a vertical pile with circular cross section. By means of the virtual work principle, the stiffness matrix of the beam element is written in terms of the solid DOFs. The beam element can thus be directly assembled with the solid element for soil–structure interaction analyses. The kinematic compatibility between beam and solid displacement fields is hence established in a weak integral form within the interaction surface. The numerical performance of the proposed elements is shown through a comparison with respect to benchmark solutions (i.e., full 3D FEM model and a semi-analytical solution).

Unlike the standard EBE, the proposed EBE formulation express all the beam DOFs (i.e., displacements as well as rotations) in terms of solid DOFs. Thus, the final equation system is expressed exclusively in terms of solid nodal parameters.

A vertical pile subjected to lateral loading is considered in order to validate the proposed formulation and compare the convergence rate of the solution with respect to a previously formulated EBE methodology. It is seen that the pile head displacements obtained by means of the proposed EBE formulation tends to the benchmark solution as the mesh size is decreased, whereas the standard EBE results do not, as stresses due to interaction forces are unbounded for decreasing mesh sizes. The internal forces (i.e., bending moments and shear forces) obtained by means of the proposed formulation are also in reasonable agreement with the benchmark solutions. This agreement is particularly remarkable for the H27B2 element. The relative error norm $||e||$ for the proposed EBE formulation

DOI: 10.1002/nag

seems to vanish for decreasing mesh sizes, for both H8B2 and H27B2 elements. As expected, the convergence rate of the H27B2 element is considerably greater than that of the H8B2 element.

Although results are shown for a single vertical pile embedded into a linear elastic soil, the proposed EBE formulation described in this paper is able to represent the soil–structure interaction phenomena in a general manner for different kinds of geotechnical problems. In this sense, nonlinear material behavior for pile, soil, or even interaction forces across the soil–pile interaction surface can be incorporated into the present model with a minor effort. This is the subject of future contributions of the authors.

The proposed formulation not only is useful for problems involving lateral loading of piles but also for any engineering application where beam-type elements (i.e., structural members for which bending and shear stiffness are relevant) need to be modeled interacting with solid elements.

ACKNOWLEDGEMENTS

The authors acknowledge the partial financial support from UTN (grant PID IN 1759), the support from SECyT UNC, and specially the PhD scholarship from CONICET, Argentina. P. J. Sánchez acknowledges the financial support from CONICET (grant PIP 2013-2015 631), Argentina, and from the European Research Council under the FP7(20072013) program (ERC grant agreement no. 320815 Advanced Grant Project on advanced tools for computational design of engineering materials COMP-DESMAT).

REFERENCES

1. Winkler E. *Die lehre von der elastizität und festigkeit (The Theory of Elasticity and Stiffness)*. H. Dominicus Prague: Czechoslovakia, 1867.
2. Vesic AS. Beams on elastic subgrade and the Winkler's hypothesis. *fifth ICSMFE* 1961; **1**:845–850.
3. Pasternak PL. *On a New Method of Analysis of an Elastic Foundation by Means of Two Constants*. Gosudarstvennoe Izdatelstvo Literaturi po Stroitelstvui Arkhitekture: Moscow, (in Russian), 1954.
4. Vlasov VZ, Leontiev UN. *Beams, Plates and Shells on Elastic Foundations*. Israel Program for Scientific Translations, Jerusalem (Translated from Russian), 1966.
5. Bittnar Z, Šejnoha J. *Numerical Methods in Structural Engineering*. ASCE: NY, 1996.
6. Poulos HG. The behavior of laterally loaded piles I): single piles. *Journal of the Soil Mechanics and Foundations Division. ASCE* 1971; **97**(sm5):711–731.
7. Randolph MF. The response of flexible piles to lateral loading. *Geotechnique* 1981; **31**(2):247–259.
8. Sadek M, Shahrour I. A three dimensional embedded beam element for reinforced geomaterials. *International Journal for Numerical and Analytical Methods in Geomechanics* 2004; **28**:931–946.
9. Bathe KJ. *Finite Element Procedures*. Klaus-Jurgen Bathe: Watertown, MA, 2006.
10. Engin HK, Septanika EG, Brinkgreve RBJ. Improved embedded beam elements for the modelling of piles. *Proc. 10th int. symp. on numerical models in geotechnical engineering–numog x, rhodes (greece)*, 2007.
11. Engin HK, Septanika EG, Brinkgreve RBJ. Estimation of pile group behavior using embedded piles. *The 12th international conference of international association for computer methods and advances in geomechanics (iacmag)*, 2008; 1–6.
12. Engin HK, Septanika EG, Brinkgreve RBJ, Bonnier PG. Modelling piled foundations by means of embedded piles. *Proceedings of the 2nd international workshop on geotechnics of soft soils, glasgow*, 2008; 131–6.
13. Randolph MF, Houlsby GT. The limiting pressure on a circular pile loaded laterally in cohesive soil. *Geotechnique* 1984; **34**(4):613–623.
14. ABAQUS Version 6.10. *User Documentation, Dassault Systemes*, 2010.

DOI: 10.1002/nag